Potential Neuroprotective Effect of Stem Cells from Apical Papilla Derived Extracellular Vesicles enriched by Lab-on-Chip approach during Retinal Degeneration

Hanieh Hadady
Royan Institue https://orcid.org/0000-0003-2447-9776
Fereshteh Karamali (frkaramali@royaninstitue.org)
Royan Institue
Fatemeh Ejeian
University of Isfahan
Sareh Sorooshzadeh
Royan Institue
Mohammad Hossein Nasr-Esfahani
Royan Institute for Biotechnology

Article

Keywords: Retinal degeneration, RCS rats, Extracellular vesicles, Stem cells from apical papilla, Micro-electromechanical device, Ultrafiltration

Posted Date: August 13th, 2021

DOI: https://doi.org/10.21203/rs.3.rs-770479/v1

Version of Record: A version of this preprint was published at Cellular and Molecular Life Sciences on May 12th, 2022. See the published version at https://doi.org/10.1007/s00018-022-04375-2.

Abstract

Retinal degeneration (RD) is recognized as a frequent cause of visual impairments, including inherited (Retinitis pigmentosa) and degenerative (age-related macular) eye diseases. Recently, dental stem cells (DSCs) have demonstrated a promising neuroprotection potential for ocular diseases through a paracrine manner carried out by extracellular vesicles (EVs). However, effective isolation of EVs is still challenging, and isolation methods determine the composition of enriched EVs and the subsequent biological and functional effects. In the present study, we assessed two enrichment methods (micro-electromechanical systems and ultrafiltration) to isolate the EVs from stem cells from apical papilla (SCAP). The size distribution of the corresponding isolates exhibited the capability of each method to enrich different subsets of EVs, which significantly impacts their biological and functional effects. We confirmed the neuroprotection and anti-inflammatory capacity of the SCAP-EVs *in vitro*. Further experiments revealed the possible therapeutic effects of subretinal injection of SCAP-EVs in the Royal College of Surgeons (RCS) rat model. We found that EVs enriched by the micro-electromechanical-based device (MEMS-EVs) preserved visual function, reduced retinal cell apoptosis, and prevented thinning of the outer nuclear layer (ONL). Interestingly, the effect of MEMS-EVs was extended to the retinal ganglion cell/nerve fiber layer (GCL/NFL). This study supports the use of the microfluidics approach to enrich valuable subsets of EVs, together with the choice of SCAP as a source to derive EVs for cell-free therapy of RD.

Introduction

A large body of evidence suggests the beneficial effects of mesenchymal stem cell (MSC) mediated therapies on retinal regeneration (RD) [1,2]. Despite the beneficial effects of cell-based therapy in regenerative medicine, undesired differentiation or malignant transformation remain concerns for clinical application [3]. Profound trophic effects of MSCs on the retina are widely accepted, and this effect is primarily mediated through paracrine signaling of the extracellular vesicles (EVs) carrying soluble retina-regulatory molecules [4,5]. EVs are small membrane-enclosed delivery vehicles that are released by the majority of the live cells and play a vital role in mediating intracellular communication through the exchange of their cargo [6]. EVs are considered a heterogonous group of particles typically categorized as exosomes (40–100 nm in diameter) and microvesicles (MVs: 0.1–1μm in diameter) [7]. According to the MISEV2018 guideline, the authors were urged to refer EV subtypes based on their size (“small EVs” (sEVs) [< 100 nm or < 200 nm] and “medium/large EVs” (m/lEVs) [> 200 nm]) instead of terms such as exosomes and MVs [8]. Emerging studies have demonstrated the therapeutic effects of stem cell-derived sEVs (mostly exosomes) on ocular diseases. In particular, subretinally injected human neural progenitor cell-derived sEVs promote photoreceptor regeneration in the Royal College of Surgeons (RCS) rats through inactivating microglia [9]. Photoreceptor protection has also been achieved after intravitreal delivery of MSC-sEVs, indicating exosomal miR-21 as a therapeutic for N-methyl-N-nitrosourea-induced retinal injury [5].

Further studies have uncovered the survival of RGCs using human embryonic [10] and bone marrow [11] stem cell-derived EVs in the optic nerve crush model.

Dental stem cells (DSCs), originally derived from neural crest cells, appear to involve in nervous system development and mediate neuroprotection [12] that may be attributed to the neurotrophic factors (such as nerve growth and brain-derived neurotrophic factors, NGF and BDNF, respectively) released by these types of cells [13,14]. Interestingly, DSCs promote paracrine-mediated neuroprotection significantly greater than human bone marrow and adipose-derived mesenchymal stem cells [15], which reportedly preserves retinal ganglion cells [16]. Stem cells from apical papilla (SCAP) originating from the cranial neural crest and found in the root apex of immature permanent teeth [17], actively contribute to their environment by producing immunosuppressive, anti-inflammatory, and trophic factors [18]. As a traditional *"biowaste"* cell source, SCAP, is a novel source of MSCs that represent a stromal cell-derived inducing activity (SDIA) to retinal cells differentiation [19] and can be considered a promising candidate for retinal regeneration [20].

The content, quality, and quantity of the EVs influence their potential bioactivity. For example, a recent study has shown that the isolation method can determine EVs' biological and functional effects at single and sub-population levels, which correlate with their composition [21]. Conventional methods of EV "enrichment", which mostly rely on concentrating, not isolating, face significant limitations, as they are often time-consuming (4-5 hours), low throughput (5–25% exosome recovery), and expensive [22–24].

Microfluidics, with the aid of an external force commonly referred to micro-electromechanical (MEMS) microfluidics, offer a rapid, efficient, and sensitive method for bio-particle manipulation [25]. Alternating current (AC) electrokinetic driven chips have been investigated for EVs capturing where electrokinetic and hydrodynamic forces work together to relocate the nanoparticles around the electrodes [26–28]. This approach offers label-free isolation and detection method in which small-medium EV enrichment occurs based on their intrinsic properties such as size, shape, and dielectric properties [29,30]. The isolation of a pure population of EVs is crucial for reliably study physiological function and biological activity. The inconsistency between studies might be one of the reasons behind the fact that very few EV-based therapeutics have progressed to clinical use. This is especially important for ocular therapeutic strategies in which a small and pure EV population is needed. Specifically, subretinal injection offers a relatively precise and direct effect on targeting cells in the subretinal space that requires a lower dose (0.1-3µl in animal studies) of therapeutic compared to intravitreal delivery (2-20µl in rats) [31–33]. Microfluidics can provide an excellent opportunity to prepare the pure EV solution for subretinal injection.

This study employed a MEMS device to enrich SCAP-derived small EVs to be injected subretinally against retinal degeneration in RCS rats. Both *in vivo* and *in vitro* confirmed potential neuroprotective effects of the MEMS enriched SCAP-EVs. It revealed that MEMS enriched SCAP-EVs inhibited apoptotic and inflammatory signal pathways in the retina by targeting *Bax*, *Bcl-2*, *Il-10*, and *Il-6*. Collectively, elucidating the potential effects of SCAP-EVs would provide promise for establishing novel therapeutics of visual loss in RD disorders.

Materials And Methods

2.1. Animals

RCS rats, regardless of sex, were provided by the Royan institute (Isfahan, IRAN) and were raised in the specific pathogen-free room of the Animal Care Center of Royan Institute, at temperatures between 20-25 °C, regular daylight exposure, and free access to food and water. The institutional research ethics committee at Royan institute (IR.ACECR.ROYAN.REC.1400.043), under the Helsinki Declaration, approved all experiments in this study. At least ten animals were used for each group.

2.2. Cell culture and conditioned medium preparation

PC12, a rat pheochromocytoma cell line, was cultured with Dulbecco's modified Eagle's medium (DMEM), 10% foetal bovine serum (FBS), 5% Horse serum, 1% L-Glutamine, 1% Nonessential amino acids (NEAA), and 1% penicillin/ streptomycin (all from Gibco, Paisley, UK). PC12 cells were seeded in a 6-well plate at a density of 8×104 cells/cm2 and cultured for 24h. Four experimental groups were defined. The H2O2 exposure group, to induce oxidative stress, was administrated with 250 µM H2O2 alone for 12 h. Two protective groups were treated with 60% SCAP-EVs (by value), enriched by ultrafiltration method (UF-EVs) and MEMS device (MEMS-EVs), 24 h before the administration of 250 µM H2O2. SCAP-EVs control group was only treated with 60% serum-reduced basal medium. To evaluate cell numbers, PC12 cells were washed with PBS, fixed in 4% PFA for 15 min at ambient temperature, stained with 4′,6-diamidino-2-phenylindole (DAPI) (Sigma, Munich, Germany), and scanned by the fluorescence microscope. For each group, cell counts were obtained from data acquisition of the 5-10 random low magnification fields of 2-3 wells using Image J software (Version 1.42q, NIH, USA).

The SCAP was acquired by Royan institute 19 and grown in standard culture conditions supplemented with DMEM, 10% FBS, 1% L-Glutamine, 1% NEAA, and 1% penicillin/ streptomycin until they reached a confluency of 70-80%. The cells were then washed three times with PBS-, dissociated using trypsin-EDTA, and 5×104 cell/ cm2 were plated in T150 flasks. One day later, the culture medium was replaced with a serum-free medium for 24 h. The collected supernatant was filtered with a 0.45-µm filter (Millipore) to discard cell debris.

2.3. EVs enrichment

The collected supernatant was loaded into the MEMS device and subsequently enriched, as previously described 34. Briefly, a 400 µL of a freshly filtered conditioned medium was placed on the chip and isolated for 20 min at 10 kHz, and peak-peak voltage 5 V. The MEMS device is composed of a MEMS layer and a polydimethylsiloxane (PDMS) chamber. The MEMS layer, which comprises two sets of interdigitated electrode arrays, connects to a function generator and produces AC electrokinetic force fields. Once the EV capture was completed, the chip was washed with a buffer (85 g/l sucrose in DI water) three times to remove bulk proteins and nucleic acids. The isolated EVs were subsequently released and collected from the chip surface by elution with PBS.

Accordingly, a freshly filtered supernatant was added to the Amicon ultra-0.5 (Millipore, 3000 MWCO) filter and centrifuged at 14000x g for 20 min. The culture medium was washed out through medium exchange with PBS. Concentrated samples were retrieved by upside-down centrifugation at 2000x g for 2 min. The concentration factor was kept consistent for both enrichment methods.

2.4. Protein content measurements

Conditioned medium was lysed by adding an equal amount of Radioimmunoprecipitation (RIPA) buffer and then incubated at 40 C for 30 min followed by 30 seconds of sonication in an ice-cold bath. Protease and phosphate inhibitors (Sigma Aldrich, Missouri, USA) were added to the lysis buffer at 1:10 concentration. Following the lysis with RIPA, total protein contents were measured using the BCA protein assay kit (KIAZIST, Kermanshah, Iran). Briefly, BSA standard or samples (5ul) were transferred to PCR tubes to which 5ul working reagent was added (working reagent 50:1 ratio of assay reagents A and B). The tubes were incubated for 30 min at 37°C, before being analyzed with Nanodrop (NANODROP 2000c, Thermo Scientific, USA).

2.5. Transmission electron microscopy (TEM)

Six microliters of conditioned medium were pipetted onto a carbon-coated grid, counterstained using 1% uranyl acetate, briefly washed with distilled water, and allowed to settle and dry for one hour at ambient temperature. To visualize the morphological characteristic of the cells releasing EVs, SCAP was fixed with 2.5% glutaraldehyde at 37°C, for 20 min. Fixed cells were then embedded in resin, sectioned using an ultra-microtome, and stained with 1% toluidine blue for visualization using light microscopy. The ultrathin sections were double-stained with 1% uranyl acetate and lead citrate. The grids were analyzed with a Philips EM208S electron microscope (FEI, The Netherlands) operating at 100 kV.

2.6. Dynamic light scattering (DLS)

EVs size distribution was evaluated by DLS experiment using a Nanoparticle sizer SZ-100 (HORIBA Scientific) performing at 90° angle.

2.7. MTS assay

The viability and metabolic activity of PC12 cells following SCAP-EVs treatment was carried out using the MTS assay by applying cell titer 96 aqueous one solution (Promega, WI, USA) according to the manufacturer's instruction. Briefly, PC12 wells from each group were incubated with MTS/PMS solution for 3.5 hours. Therefore, the insoluble formazan crystals were dissolved, and the absorbance of the resulting colored solution was measured at 492 nm exploiting a micro-plate reader (AWARNESS Technology, Inc., USA) and normalized to the cell-free solution.

2.8. Subretinal transplantation

All animals were divided into three groups with ten individuals at least. The animals were anesthetized by intraperitoneal injection of ketamine (50 mg/kg) and xylazine (5mg/kg). The right eyes were enrolled in this study. Subretinal transplantations were performed in RCS rats (postnatal 21 days) with UF-EVs, MEMS-EVs, or unconditioned basal medium (vehicle). The retinas that did not receive any injections were the untreated control group. The right eye of RCS rats was injected with 2 µL concentrated SCAP-EVs resuspended solution that contained 4µg protein, which is approximately equivalent to 1.76 ± 0.2 e 09 sEVs 35. The subretinal transplantation method was adapted from Ben M'Barek et al.36. Briefly, a local subretinal detachment was created through air injection via an insulin syringe under an operating microscope (OMS-90) following a small sclera incision. Generating a hole into the cornea reduced the intraocular pressure. After the subretinal injection of the solution, the syringe was held in place for 30 seconds to prevent any leakage. The animals exhibiting any complications such as massive intraocular, retinal hemorrhage, or endophthalmitis after surgery were excluded from the study.

2.9. TUNEL staining

Apoptotic cells of the retina were detected using in situ cell death detection kit (DeadEnd™ Fluorometric TUNEL System kit, Promega, Madison, WI) and PI counterstain (Sigma-Aldrich, USA) according to the manufacturer's protocol. All slides were visualized under a fluorescent microscope (Olympus, Center Valley, PA, USA) equipped with an Olympus DP70 camera.

2.10. Histological assessment

RCS rats were euthanized on day 28 after transplantation by carbon dioxide inhalation, and right eyes were enucleated for further analysis. These eyecups were fixed in 4% PFA overnight at 4°C. Sections (4 µm thickness) were cut from tissue that is embedded in paraffin wax, attached to glass slides perpendicular to the optic disc, and stained with hematoxylin and eosin (H&E) for light microscopy. For all eyes, the sections were obtained at the same distance (1600 µm) from the iris. Z-projected thickness and nucleus count of outer nuclear and ganglion cell layers (ONL and GCL, respectively) were analyzed by Image J. The retinal neovascularization was evaluated by H&E staining of the RCS rat eyes three months after transplantation. The average number of intravitreal vessels per section was determined by counting the vascular lumens on the vitreous side of the inner limiting membrane. Three independent experiments were considered for all corresponding groups (UF-EVs, MEMS-EVs, vehicle, and control). The untreated left eyes were assigned as the control group.

2.11. Immunofluorescence staining (IF)

Heat-induced antigen retrieval was first carried out by autoclaving sections in citrate buffer (sodium citrate–citric acid) at pH 6.0. All slides were then air-dried, washed in PBS, and incubated with primary antibodies (diluted into 10% normal goat serum (Sigma, Munich, Germany)) at 4º C overnight. Following two wash steps with PBS, the sections were incubated with secondary antibodies (diluted into 5% normal goat serum) at 37°C for 1h, counterstained with DAPI or PI, and scanned and photographed via fluorescence microscopy. The antibodies and dilutions that have been used in our study are as follow:

CD81 (Cat. No. Sc7637, Santa Cruz, 1:50), Anti-PCNA (Cat. No. Ab29, Abcam, 1:50), Anti-Rhodopsin (Cat. No. Ab81702, Abcam, 1:50), Goat Anti-mouse IgG TRITC (Cat. No. T7882, Sigma, 1:60), Goat Anti-mouse-FITC (Cat. No. AP124F, Sigma, 1:200).

2.12. Flow cytometry

For identification, enriched EVs were incubated with CD81 antibody (as described above) for 1 hour at 37 º C in the dark and mixed every 10 min. A parallel sample with an isotype control antibody was incubated under the same condition to control the nonspecific binding. The gates were positioned and calibrated using 300-nm beads.

2.13. Reverse-transcription quantitative polymerase chain reaction (RT-qPCR) analysis

The retinal layer of the enucleated eyes was isolated mechanically under dissecting stereomicroscope. Total RNA of the PC12 cells and isolated retina was extracted using TRIzol reagent as the manufacturer's instructions. Biotechrabbit™ Kit (Cat. No. BR0400403, Germany) was used to transcribe RNA to cDNA as the manufacturer's instructions. Expression levels of the apoptotic and inflammatory mediated genes were measured with RT-qPCR. Normalizing to GAPDH levels, all expression values were calculated using the comparative threshold cycle method (ΔΔCT). The mean and standard deviations were computed from four independent experiments. The sequences of primer pairs that are used in this study are as follow:

Bcl-2:

FP: 5-$AC\top CTCTCGTCGCTA\mathbb{C}$; RP: 5-AAGAGTTCCTCCACCACCGT-3

Bax:

FP: 5-GGATCGAGCAGAGAGGATGG-3; RP: 5-ACACTCGCTCAGCTTCTTGG-3

Il-6:

FP: 5-GAACAACTTACAAGATAACA-3; RP: 5-GACTCTAACTTCTCCATTA-3

Il-10:

FP: 5-AGCAGGTGAAGAATGATT-3; RP: 5-GCAGTTGATGAAGATGTC-3

GAPDH:

FP: 5-TGCCGCCTGGAGAAACC-3; RP: 5-TGAAGTCGCAGGAGACAACC-3

2.14. Visual cliff avoidance test

Visual function of the RCS rats at day 28 post-operation was evaluated using a depth perception visual cliff, as previously described 37. In brief, rats were placed on a stage at the center of a Perspex platform, which creates an appearance of a cliff. Animal's activity was recorded for 2 min with a phone camera, and the latency to dismount the stage (in seconds) was analyzed. Ten individuals per group (30 total) were tested once (for each rat) to avoid the memory effect.

2.15. Statistical analysis

All data were presented as the mean ± SE (standard error of the mean) from at least three biological samples for each test and ten for each group. Statistical differences were calculated using one-way analysis of variance (ANOVA) for comparison between two groups and Dunnett or Sidak tests to compare multiple groups. P values < 0.05 were considered to be significant.

Results

3.1 SCAP releases EVs into the extracellular environment

Cells constitutively release EVs during cell-cell communication. In this study, the SCAP, with a homogenous spindle-shaped morphology (Figure 1a), was used as the parent cells to drive EVs. Figure 1b-d reveal the secretion and ultrastructural morphology of SCAP-derived EVs using TEM. Electron micrographs show EVs biogenesis that involves fusing multivesicular bodies (MVB) (Figure 1b) with the plasma membrane and subsequent release of a heterogeneous population of membrane-bilayered vesicles with different sizes (Figure 1c, d). MVB can either fuse with lysosomes to degrade their cargo or with the plasma membrane to release their cargo extracellularly (Figure S1). To enrich EVs, we first collected SCAP conditioned medium according to a standard workflow (Figure 1e). We further examined EVs' presence in the collected conditioned medium using TEM and flow cytometry. TEM showed that SCAP-derived EVs exhibited typical cup-shaped bilayer membrane vesicles with diameters ranging from 50 to 300 nm (Figure 1f, insert box). Phenotype characterization by flow cytometry confirmed the expression of the CD81, a feature biomarker of EVs (Figure 1g).

3.2 Enrichment method determines the functional effect of EVs

To investigate the functionality of EVs, we employed two enrichment methods, including ultrafiltration (UF-EVs) and MEMS microfluidics (MEMS-EVs). The isolation principles are based on size exclusion forced by AC electrokinetic relocation for MEMS method and sedimentation pressure for UF method as demonstrated in Figures 2a and b, respectively. Our previous work found that the proposed MEMS device captured sEVs at 10kHz frequency and 5Vpp 34. We analyzed the enrichment capacity of the MEMS device at two frequencies (10 kHz and 100 kHz) and three isolation periods (10 min, 20 min ad 40 min) by BCA protein assay. For each column, the protein recovery efficiency (%) was measured as follow:

Protein recovery efficiency (%)=((protein concentration after enrichment)⁄(protein concentration before enrichment))×100

To recover the concentrate once the EV capture was completed, the MEMS device was washed with 300 µL of elution buffer (85 g/l sucrose in DI water) to remove bulk proteins and nucleic acids, and then the isolated EVs were repelled from the chip surface by elution with PBS. The highest EVs' yield was obtained after 20 min isolation at 10 kHz frequency (Figure 2c). The size analysis by DLS showed that isolates produced by ultrafiltration contained larger vesicles (an average of 272 nm) with fairly similar protein recovery (72% for UF method compared to 74% for MEMS method) evaluated by BCA protein assay while isolates produced by MEMS method contained smaller vesicles (an average of 46nm) (Figure 2d).

3.3 Functional inhibition of apoptosis and inflammation signal pathways by SCAP-EVs protect PC12 cells exposed to H2O2 in vitro

To investigate the neuroprotection effect of SCAP-EVs, we employed H2O2-induced oxidative stress in cultured PC12 cells as an in vitro model and evaluated whether pretreatment of PC12 cells with SCAP-EVs that are enriched by both methods could inhibit the cytotoxic effects of H2O2 (Figure 3a). Serum content was reduced to replace it with SCAP-EVs. The viability changes were normalized as percentages of the control, unexposed cells and plotted against various concentrations. There was no significant difference in the viability of PC12 cells between the control group (100% serum content by value) and 40%, 50%, and 60% serum reduced groups (Figure S2a). Therefore, 60% of the serum content was replaced with enriched SCAP-EVs groups. The dose-response curve of H2O2 exposure after 12 hours was calculated with an IC50 (the half-maximal inhibitory concentration) of ≅250 µM (Figure S2b).

Metabolic activity of the PC12 cells cultured in 60% serum reduced medium was not changed significantly compared to the control group, implying that cell viability was not affected by 60% depletion of serum content for 24h (Figure 3b). While, the viability of PC12 cells in the 250 µM H2O2 exposure group was significantly lower than that in the serum-reduced control group. Furthermore, the reduced viability of PC12 cells exposed to H2O2 was recovered to about 13%, and 66% in groups that were pretreated with UF and MEMS enriched SCAP-EVs, respectively. To confirm the protective effect, we assessed the cell numbers using DAPI staining and data analysis. Cell count quantification revealed a greater number of the cells in the MEMS-EVs group than the controls and UF-EVs (Figure 3c, d).

As it is well known that MSCs have the capacity to modulate the inflammatory and apoptosis responses 38, we further examined the expression of pro/anti-inflammatory (Il-6, Il-10) and pro/anti-apoptosis (Bax, Bcl-2) cytokines under H2O2 and SCAP-EVs treatments at mRNA level with qRT-PCR. H2O2 stimulation markedly decreased Il-10 and Bcl-2 mRNA levels and increased Il-6 and Bax mRNA levels compared to the control group, while MEMS-EVs treatment reversed the effect of H2O2 stimulation (Figure 3e). These results suggest that SCAP-EVs suppress the H2O2-induced cytotoxic effect in vitro. However, the in vitro modulatory potential of UF-EVs against the H2O2 stimulation is statistically significant just for Il-6 and Bax cytokines.

3.4 SCAP derived EVs modulate inflammation and apoptosis to preserve visual function in RCS rats

To evaluate whether SCAP-EVs exerted therapeutic effects during retinal degeneration in RCS rats and further define the underlying mechanism, we performed in vivo experiments (Figure 4a). To meet this goal, we injected 2 μL SCAP-EVs enriched by both UF and MEMS methods into the subretinal space of the RCS rats. The 2 μL concentrates approximately contained 4μg protein according to the BCA protein assay. The left eye served as an untreated group for comparison. Visual function assessment using visual cliff test showed that MEMS-EVs treatment rescued the visual acuity of RCS rats 28 days post-injection, compared with the vehicle and UF-EVs (Figure 4b). The expression of pro/anti-inflammatory (Il-6, Il-10) and pro/anti-apoptosis (Bax, Bcl-2) cytokines under enriched SCAP-EVs treatment at mRNA level with qRT-PCR reveal that MEMS-EVs treatment markedly up-regulated the levels of Il-10 and Bcl-2 mRNA expressions and down-regulated the levels of Il-6 and Bax mRNA expressions, compared to the vehicle (Figure 4c).

It has been reported that genetic mutation results in apoptosis of photoreceptors and reduction in thickness of ONL in RCS rats 39. TUNEL staining showed that the MEMS-EVs group significantly reduced the number of apoptotic cells in the ONL of RCS rats, compared with the untreated control, vehicle group, and the UF-EVs treated eyes at days 28 post-injection (Figure 4d, e), which is consistent with the anti-apoptotic results in Figure 4c.

In the RCS rat, the retinal pigment epithelium (RPE) cells are not phagocytizing the rod outer segment (OS) debris 39. Moreover, the OS became disorganized, and the ONL was reduced to a single layer of cells that are associated with an autofluorescence debris zone 40. Therefore, photoreceptor regeneration could be one of the mechanisms that mediate the observed protective effects, as previously described 36,41. To confirm the potential of SCAP-EVs for photoreceptor regeneration, we examined rhodopsin protein expression (Figure 5). Rhodopsin staining exhibited OS disappearance of rod photoreceptors in untreated control and vehicle, whereas rhodopsin-positive surface was markedly increased in the MEMS-EVs group. Although UF-EVs group showed an improved effect, the difference is not statistically significant. These results demonstrate that SCAP-EVs that are particularly enriched by the MEMS method preserves the photoreceptors from apoptosis and modulate the inflammatory response to protect the visual function in an RD model.

3.5 SCAP derived EVs preserve retinal morphology in RCS rats

To evaluate the morphology of the retinal layers post-injection, we performed H&E and proliferating cell nuclear antigen (PCNA) staining (white arrowhead). We did not find uncontrolled cell proliferation expressed PCNA in the retinal cross-sections of the RCS that had received SCAP-EVs (Figure S3). Morphologically, the ONL thickness was preserved significantly in the MEMS-EVs group, compared with that in untreated control, vehicle, and UF-EVs with relatively similar thicknesses (Figure 6a, b). Interestingly, the retinal nerve fiber layer (NFL) thickness, which is a measure of RGC axonal density, increased in animals receiving MEMS-EVs (Figure 6c). The numbers of cells in ONL and GCL

corresponding layers suggest that cell bodies are also affected during treatment with SCAP-EVs (Figure 6 d, e).

We observed that the retinal thickness increased around the injected area in the MEMS-EVs group compared with the untreated control, vehicle, and UF-EVs groups, as previously described 9 (Figure S4).

3.6. SCAP derived EVs did not promote neovascularization in RCS rats

We further assessed the angiogenesis effect of SCAP-EVs three months after transplantation in RCS rats. There is no statistically significant difference among the average number of vascular lumens counted on the vitreous side of the boundary between the retina and the vitreous body in the MEMS-EVs and UF-EVs compared to vehicle and untreated groups (Figure S5).

Discussion

Transplantation of DSCs is a promising therapeutic approach for neurodegenerative disorders, including retinal degeneration (RD) [42,43]. Of particular importance to this purpose, DSC-EVs could be an effective therapy and potentially avoid the drawbacks of stem cell therapy, including probable immune response and ethical issues. Recent studies have reported diverse biomedical function activity for dental pulp stem cells-derived EVs in animal models, including anti-apoptotic, hematopoietic recovery, and bone regeneration capacity [44,45]. Treatment of the RCS rats by EVs derived from human embryonic [46] and neural progenitor cells [9] have proved to be therapeutically efficacious via microRNA exchange. These previous studies possess similarities to our findings and help us better understand the underlying mechanism in RD treatment. The present study aimed to introduce SCAP as a novel source of EVs with substantial neuroprotective potential that is particularly advantageous at the early stages of RD treatment. We confirmed through visual cliff testing that subretinal delivery of SCAP-EVs preserved the visual function of the RCS rats. Another aspect of the novelty of this work lies in the micro-electromechanical microfluidics (MEMS) device that we exploit to enrich the precise population of small EVs. Our previous work characterized and designed the MEMS device capable of enrichment of sEVs [34]. Briefly, this device offers a label-free and relatively fast method to isolate and enrich particles using AC electrokinetic phenomena. When placed in an AC electric field, a particle will polarize (i.e., develop a dipole moment) dependent on the intrinsic properties of the particle, such as dielectric properties, size, and shape. Therefore MEMS microfluidics approach was utilized to enrich EVs using the AC electrokinetic net force to relocate the EVs laterally within a chamber where the target population is pulled away from the rest of the population. This method could serve as a novel, precise enrichment method, particularly for ocular treatment, as it mainly requires a small and effective dose of therapeutics.

EVs, as a heterogeneous group of cell-derived nanoparticles, include several subtypes that share similar size and morphology, making it difficult to differentiate. Research is still ongoing to decipher whether and how each subset mediates the diverse biological effects. Here, we discovered that SCAP-EVs, which are enriched by the MEMS method, demonstrate a neuroprotective effect as well as the capacity to alleviate

the RD in the RCS model. We further observed that UF-EVs revealed a partial therapeutic capacity *in vitro*, though the difference between protective effects of MEMS and UF enrichment methods was more prominent *in vivo*, most likely due to the diverse biological capabilities of EVs subsets. We also found that MEMS-EVs mostly contained sEVs subsets, although both UF and MEMS methods seemed to have a relatively similar protein recovery. Moreover, compressible and deformable particles such as EVs can be pushed through the membrane pores due to the applied driving force even if they are larger than the pore size [47]. Therefore, the UF method is associated with partial particle loss, presumably the sEVs subsets.

RD and ultimate vision loss is aligned with retinal cells death, especially photoreceptors, due to the multiple mechanisms [48]. Moreover, retinal neuroinflammation begins at the early stages of RD and is amplified at advanced stages. Therefore, the inflammatory modulation response seems to be a critical factor for the success of retinal regeneration therapies [49]. Importantly, SCAP can secrete a large variety of neuroprotective and immunomodulatory factors with a higher capacity to conventional MSC origins, making them a desirable candidate for neural regeneration [13]. Given that PC12 cells are neural progenitor cells and considered a major model system to study many aspects of neuronal activity [50], we employed H2O2-induced oxidative stress in cultured PC12 cells as an *in vitro* model and evaluated neuroprotection and anti-inflammatory response in cells pretreated with SCAP-EVs. We found that the MEMS-EVs group, particularly, revealed a higher anti-apoptosis and anti-inflammatory response that confirmed the therapeutic effect of MEMS-EVs against neuroinflammation.

Previous studies have thoroughly documented that the RCS rats have a mutation in the merTK gene that ultimately leads to photoreceptor cell death to such an extent that at seven weeks of age, almost half of the nuclei of the photoreceptors have degenerated [39]. Moreover, the genetic mutation prevents RPE phagocytosis of photoreceptors shed outer segments, leading to a disorganized OS and a thinner ONL [39]. It has been reported that dental pulp stem cells have the capability to respond to cues from the retina and express mature photoreceptor marker rhodopsin *ex vivo* [51]. In the present study, we observed that the ONL of the MEMS-EVs group had fewer apoptotic cells compared to the untreated control, vehicle, and UF-EVs treated groups. Furthermore, immunohistochemical staining for the photoreceptor cell markers rhodopsin confirmed more rhodopsin-positive OS in rat eyes treated with MEMS-EVs compared to untreated control, vehicle, and UF-EVs treated groups. These results support the notion that conservation of the visual acuity in the MEMS-EVs treated eyes was correlated with the preservation of photoreceptors in the ONL, identified by rhodopsin expression in the OS of photoreceptors, and observed anti-apoptotic response. Morphologically, MEMS-EVs increased the cell nuclei density and delayed the thinning of ONL and GCL/NFL. However, the numbers of retinal cells labelled with the proliferating cell nuclear antigen (PCNA) were not significantly different among the control and protective groups, reflecting that majority of retinal cells did not proliferate, not even in the presence of SCAP-EVs, but when SCAP-EVs were present, the survival or anti-apoptotic pathways were promoted. These data are in line with previous neuroprotection studies that aim to preserve retinal cells' viability in the early stage of vision loss and postpone the development of retinal degeneration [52]. Angiogenic factors such as vascular endothelial growth factor (VEGF), which stimulate neovascularization in the pathological processes, are closely involved in RD

pathogenesis [53,54]. However, profiling SCAP secretion capacity exhibited that SCAP conditioned medium and EVs could potentially promote angiogenesis [18,55]. It has been shown that microenvironmental cues present in damaged tissue may induce endothelial transdifferentiation of SCAP, enhancing their regeneration potential [56]. Therefore the effect of SCAP-EVs on neovascularization has to be studied before taking any further steps toward the clinic. Our quantitative assessment of the retinal neovascularization three months after transplantation revealed no statistically significant difference among the average count of vascular lumens in protective groups compared to the control groups giving insight into the neovascularization property of SCAP-EVs.

To further evaluate the underlying protective mechanisms of SCAP-EVs, we sought to evaluate the inflammatory and apoptotic-related marker expressions (*Il-10*, *Il-6*, *Bax,* and *Bcl-2*). In agreement with the previous immunohistochemical results, we found suitable therapeutic functionality via regulation of apoptotic-related factors (*Bax* and *Bcl-2*) in the MEMS-EVs treated group compared to the vehicle. Moreover, we detected the up-regulation of *Il-10* and down-regulation of *Il-6*, indicating the anti-inflammatory response of the MEMS-EVs treated group compared to the vehicle, which is in line with the reported neuroprotective potential of these cells [20].

On the whole, our data suggest that SCAP-EVs mediate neuroprotection in the RD model through mitigation of apoptosis and inflammation responses. MEMS enrichment method is capable of isolating a smaller and effective EVs population that protects the visual acuity, reinforcing the notion that EVs' isolation methods determine the compositions and therapeutic capacity of the isolates. These endeavors are crucial for a wide range of biomedical and clinical applications as a remarkable practical and vital candidate since a MEMS device can be employed to generate patient-specific (personalized medicine) therapeutics. Our findings suggest that SCAP-EVs is potentially a promising candidate for RD treatment.

References

1. Ding, S. S. L., Subbiah, S. K., Khan, M. S. A., Farhana, A. & Mok, P. L. Empowering mesenchymal stem cells for ocular degenerative disorders. *International Journal of Molecular Sciences* vol. 20 (2019).

2. Adak, S., Magdalene, D., Deshmukh, S., Das, D. & Jaganathan, B. G. A Review on Mesenchymal Stem Cells for Treatment of Retinal Diseases. *Stem Cell Reviews and Reports* (2021) doi:10.1007/s12015-020-10090-x.

3. Volarevic, V. *et al.* Ethical and safety issues of stem cell-based therapy. *International Journal of Medical Sciences* vol. 15 36–45 (2018).

4. Yu, B., Li, X. R. & Zhang, X. M. Mesenchymal stem cell-derived extracellular vesicles as a new therapeutic strategy for ocular diseases. *World J. Stem Cells* **12**, 178–187 (2020).

5. Deng, C. L. *et al.* Photoreceptor protection by mesenchymal stem cell transplantation identifies exosomal MiR-21 as a therapeutic for retinal degeneration. *Cell Death Differ.* **28**, 1041–1061 (2020).

6. Yang, B., Chen, Y. & Shi, J. Exosome Biochemistry and Advanced Nanotechnology for Next-Generation Theranostic Platforms. *Adv Mater* **31**, e1802896 (2019).

7. Pegtel, D. M. & Gould, S. J. Exosomes. *Annu Rev Biochem* **88**, 487–514 (2019).

8. Théry, C. *et al.* Minimal information for studies of extracellular vesicles 2018 (MISEV2018): a position statement of the International Society for Extracellular Vesicles and update of the MISEV2014 guidelines. *J. Extracell. Vesicles* **7**, (2018).

9. Bian, B. *et al.* Exosomes derived from neural progenitor cells preserve photoreceptors during retinal degeneration by inactivating microglia. *J. Extracell. Vesicles* **9**, 1748931 (2020).

10. Seyedrazizadeh, S. Z. *et al.* Extracellular vesicles derived from human ES-MSCs protect retinal ganglion cells and preserve retinal function in a rodent model of optic nerve injury. *Stem Cell Res. Ther.* **11**, 203 (2020).

11. Mead, B. & Tomarev, S. Bone marrow-derived mesenchymal stem cells-derived exosomes promote survival of retinal ganglion cells through mirna-dependent mechanisms. *Stem Cells Transl. Med.* **6**, 1273–1285 (2017).

12. Luo, L. *et al.* Potential roles of dental pulp stem cells in neural regeneration and repair. *Stem Cells International* vol. 2018 (2018).

13. Kolar, M. K. *et al.* The neurotrophic effects of different human dental mesenchymal stem cells. *Sci. Rep.* **7**, 1–12 (2017).

14. De Almeida, J. F. A., Chen, P., Henry, M. A. & Diogenes, A. Stem cells of the apical papilla regulate trigeminal neurite outgrowth and targeting through a BDNF-dependent mechanism. *Tissue Eng. - Part A* **20**, 3089–3100 (2014).

15. Mead, B., Logan, A., Berry, M., Leadbeater, W. & Scheven, B. A. Paracrine-mediated neuroprotection and neuritogenesis of axotomised retinal ganglion cells by human dental pulp stem cells: Comparison with human bone marrow and adipose-derived mesenchymal stem cells. *PLoS One* **9**, (2014).

16. Mead, B., Logan, A., Berry, M., Leadbeater, W. & Scheven, B. A. Intravitreally transplanted dental pulp stem cells promote neuroprotection and axon regeneration of retinal ganglion cells after optic nerve injury. *Investig. Ophthalmol. Vis. Sci.* **54**, 7544–7556 (2013).

17. Sonoyama, W. *et al.* Characterization of the Apical Papilla and Its Residing Stem Cells from Human Immature Permanent Teeth: A Pilot Study. *J. Endod.* **34**, 166–171 (2008).

18. Yu, S., Zhao, Y., Ma, Y. & Ge, L. Profiling the secretome of human stem cells from dental apical papilla. *Stem Cells Dev.* **25**, 499–508 (2016).

19. Karamali, F., Esfahani, M. H. N., Taleahmad, S., Satarian, L. & Baharvand, H. Stem cells from apical papilla promote differentiation of human pluripotent stem cells towards retinal cells. *Differentiation* **101**, 8–15 (2018).

20. Kang, J., Fan, W., Deng, Q., He, H. & Huang, F. Stem Cells from the Apical Papilla: A Promising Source for Stem Cell-Based Therapy. *BioMed Research International* vol. 2019 (2019).

21. Huyen Phan, T. *et al.* New multiscale characterisation methodology for effective determination of isolation-structure-function relationship of extracellular vesicles. *bioRxiv* 2021.02.09.430523 (2021) doi:10.1101/2021.02.09.430523.

22. Lamparski, H. G. *et al.* Production and characterization of clinical grade exosomes derived from dendritic cells. *J. Immunol. Methods* **270**, 211–226 (2002).

23. Webber, J. & Clayton, A. How pure are your vesicles? *J. Extracell. Vesicles* **2**, (2013).

24. Momen-Heravi, F. *et al.* Current methods for the isolation of extracellular vesicles. *Biological Chemistry* vol. 394 1253–1262 (2013).

25. Islam, N. & Saye, S. MEMS Microfluidics for Lab-on-a-Chip Applications. in *Microelectromechanical Systems and Devices* (InTech, 2012). doi:10.5772/39206.

26. Chen, J. *et al.* Rapid and efficient isolation and detection of extracellular vesicles from plasma for lung cancer diagnosis. *Lab Chip* **19**, 432–443 (2019).

27. Ibsen, S. D. *et al.* Rapid Isolation and Detection of Exosomes and Associated Biomarkers from Plasma. *ACS Nano* **11**, 6641–6651 (2017).

28. Lewis, J. M. *et al.* Integrated Analysis of Exosomal Protein Biomarkers on Alternating Current Electrokinetic Chips Enables Rapid Detection of Pancreatic Cancer in Patient Blood. *ACS Nano* **12**, 3311–3320 (2018).

29. Hadady, H., Wong, J. J., Hiibel, S. R., Redelman, D. & Geiger, E. J. High frequency dielectrophoretic response of microalgae over time. *Electrophoresis* **35**, (2014).

30. Ramos, A., Morgan, H., Green, N. G. & Castellanos, A. Ac electrokinetics: a review of forces in microelectrode structures. *J. Phys. D Appl. Phys.* **31**, 2338–2353 (1998).

31. Peng, Y., Tang, L. & Zhou, Y. Subretinal Injection: A Review on the Novel Route of Therapeutic Delivery for Vitreoretinal Diseases. *Ophthalmic Res.* **58**, 217–226 (2017).

32. Dureau, P. *et al.* Quantitative analysis of subretinal injections in the rat. *Graefe's Arch. Clin. Exp. Ophthalmol.* **238**, 608–614 (2000).

33. Vezina, M. *et al.* Determination of Injectable Intravitreous Volumes in Rats. *ARVO Annu. Meet. Abstr.* 1–2 (2011).

34. Hadady, H. *et al.* AC electrokinetic isolation and detection of extracellular vesicles from dental pulp stem cells: Theoretical simulation incorporating fluid mechanics. *Electrophoresis* elps.202000376 (2021) doi:10.1002/elps.202000376.

35. Wang, J., Bonacquisti, E. E., Brown, A. D. & Nguyen, J. Boosting the Biogenesis and Secretion of Mesenchymal Stem Cell-Derived Exosomes. *Cells* **9**, 660 (2020).

36. M'Barek, K. Ben *et al.* Human ESC–derived retinal epithelial cell sheets potentiate rescue of photoreceptor cell loss in rats with retinal degeneration. *Sci. Transl. Med.* **9**, (2017).

37. Tzameret, A. *et al.* Evaluation of visual function in Royal College of Surgeon rats using a depth perception visual cliff test. *Vis. Neurosci.* **36**, (2019).

38. Fan, X. L., Zhang, Y., Li, X. & Fu, Q. L. Mechanisms underlying the protective effects of mesenchymal stem cell-based therapy. *Cellular and Molecular Life Sciences* vol. 77 2771–2794 (2020).

39. Ryals, R. C. *et al.* Long-term characterization of retinal degeneration in royal college of surgeons rats using spectral-domain optical coherence tomography. *Investig. Ophthalmol. Vis. Sci.* **58**, 1378–1386 (2017).

40. Carr, A.-J. *et al.* Protective Effects of Human iPS-Derived Retinal Pigment Epithelium Cell Transplantation in the Retinal Dystrophic Rat. *PLoS One* **4**, e8152 (2009).

41. Dai, J., Fu, Y., Zeng, Y., Li, S. & Qin Yin, Z. Improved retinal function in RCS rats after suppressing the over-activation of mGluR5. *Sci. Rep.* **7**, 1–14 (2017).

42. Luzuriaga, J. *et al.* Advances and perspectives in dental pulp stem cell based neuroregeneration therapies. *International Journal of Molecular Sciences* vol. 22 3546 (2021).

43. Abuarqoub, D. *et al.* Neuro-regenerative potential of dental stem cells: a concise review. *Cell and Tissue Research* vol. 382 267–279 (2020).

44. Imanishi, Y. *et al.* Efficacy of extracellular vesicles from dental pulp stem cells for bone regeneration in rat calvarial bone defects. *Inflamm. Regen.* **41**, 12 (2021).

45. Kong, F. *et al.* Dental Pulp Stem Cell-Derived Extracellular Vesicles Mitigate Haematopoietic Damage after Radiation. *Stem Cell Rev. Reports* **17**, 318–331 (2021).

46. Ke, Y. *et al.* Human embryonic stem cell-derived extracellular vesicles alleviate retinal degeneration by upregulating Oct4 to promote retinal Müller cell retrodifferentiation via HSP90. *Stem Cell Res. Ther.* **12**, 21 (2021).

47. Woods, J., Pellegrino, J. & Burch, J. Generalized guidance for considering pore-size distribution in membrane distillation. *J. Memb. Sci.* **368**, 124–133 (2011).

48. Wenzel, A., Grimm, C., Samardzija, M. & Remé, C. E. Molecular mechanisms of light-induced photoreceptor apoptosis and neuroprotection for retinal degeneration. *Progress in Retinal and Eye Research* vol. 24 275–306 (2005).

49. Noailles, A. *et al.* Persistent inflammatory state after photoreceptor loss in an animal model of retinal degeneration. *Sci. Rep.* **6**, 1–16 (2016).

50. Zhang, S., Ye, J. & Dong, G. Neuroprotective effect of baicalein on hydrogen peroxide-mediated oxidative stress and mitochondrial dysfunction in PC12 cells. *J. Mol. Neurosci.* **40**, 311–320 (2010).

51. Bray, A. F., Cevallos, R. R., Gazarian, K. & Lamas, M. Human dental pulp stem cells respond to cues from the rat retina and differentiate to express the retinal neuronal marker rhodopsin. *Neuroscience* **280**, 142–155 (2014).

52. Pardue, M. T. & Allen, R. S. Neuroprotective strategies for retinal disease. *Progress in Retinal and Eye Research* vol. 65 50–76 (2018).

53. Cabral, T. *et al.* Retinal and choroidal angiogenesis: A review of new targets. *International Journal of Retina and Vitreous* vol. 3 31 (2017).

54. Paulus, Y. M. & Sodhi, A. Anti-angiogenic therapy for retinal disease. in *Handbook of Experimental Pharmacology* vol. 242 271–307 (Springer New York LLC, 2017).

55. Liu, Y. *et al.* Exosomes derived from stem cells from apical papilla promote craniofacial soft tissue regeneration by enhancing Cdc42-mediated vascularization. *Stem Cell Res. Ther.* **12**, 1–14 (2021).

56. Bakopoulou, A. *et al.* Angiogenic Potential and Secretome of Human Apical Papilla Mesenchymal Stem Cells in Various Stress Microenvironments. *Stem Cells Dev.* **24**, 2496–2512 (2015).

Figures

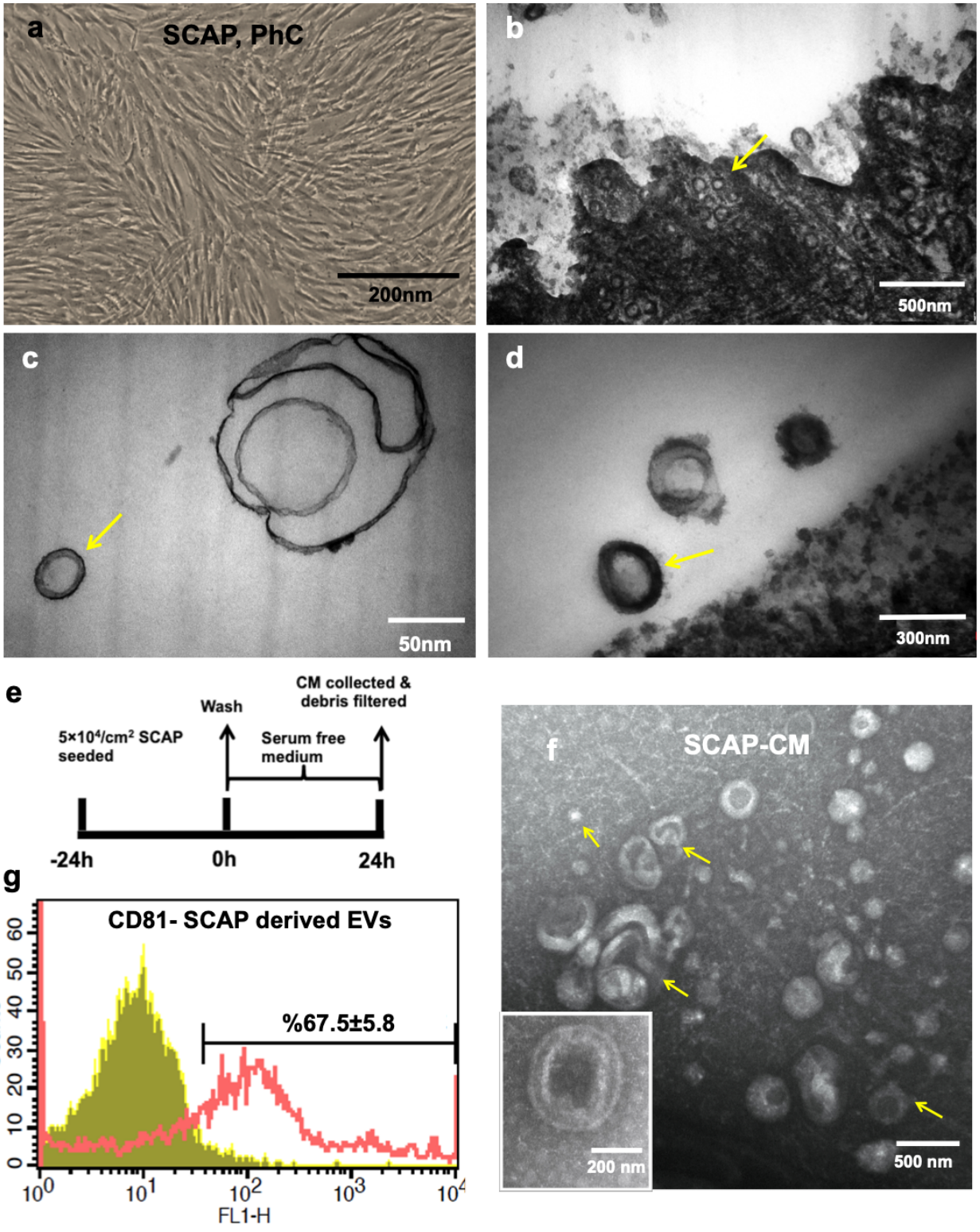

Figure 1

SCAP as a source to derive EVs (a) Bright-field (phase contrast) image of homogenous spindle-shaped SCAP, (b) Electron micrograph of SCAP ultrastructure; arrows show MVB containing EVs, (c) sEVs: small (30-110 nm), (d) m/lEVs: medium to large (100-1000 nm), (e) Experimental workflow of conditioned medium collection, (f) Electron micrograph of conditioned medium indicating a heterogenous population of EVs, (g) Flow cytometry analysis of SCAP conditioned medium, The area under the pink line identifies

EVs reacting with CD81. The area under the yellow line indicates the interactions of EVs with corresponding non-reactive immunoglobulin of the same isotype. Abbreviations: MVB, Multivesicular bodies; CM, Conditioned medium

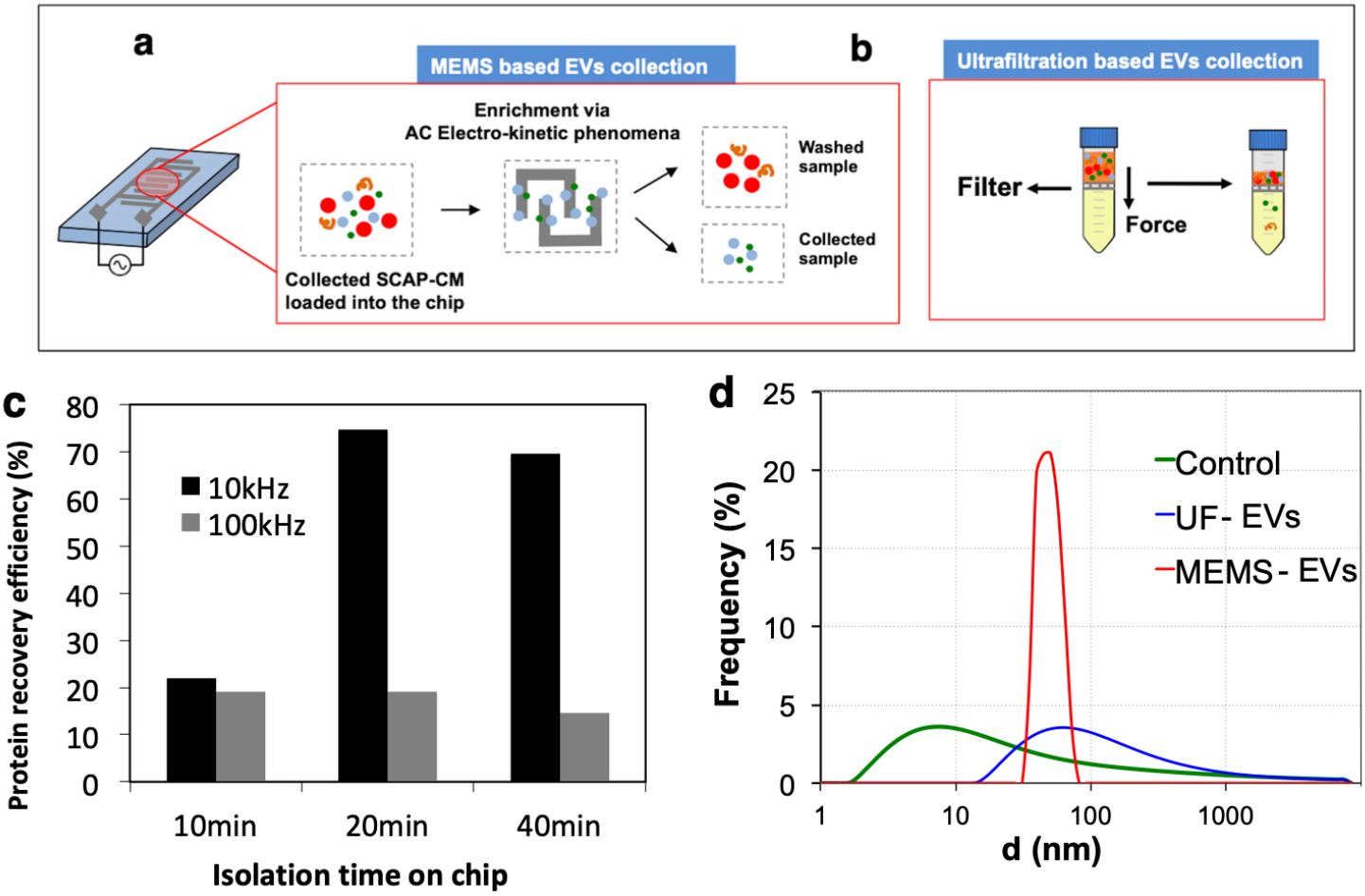

Figure 2

The principles of EVs enrichment approaches (a) MEMS-based EVs collection: briefly, particles that are spiked into a low conductivity medium and have similar size, shape, and intrinsic dielectric properties trap around the edge of the electrodes and along its surface under the influence of AC electrokinetic forces. Entrapment occurred at a specified 10 kHz AC frequency and 5 Vpp. (b) Ultrafiltration-based EVs collection: sedimentation pressure forced particles to pass through a filter with particular pore size. In this study, a regenerated cellulose filter with 3KD cut-off was employed. (c) Protein recovery efficiency (%) [(Protein concentration after enrichment/Protein concentration before enrichment) * 100] of the MEMS method, (d) Size distribution of each isolation method: green line indicates the size distribution of the UF EVs isolates, the red line indicates the size distribution of MEMS method, the blue line indicates the size distribution of the conditioned medium before the enrichment. Abbreviation: MEMS, Micro-electromechanical systems; Vpp, Voltage peak to peak; AC, Alternative current; UF, Ultrafiltration

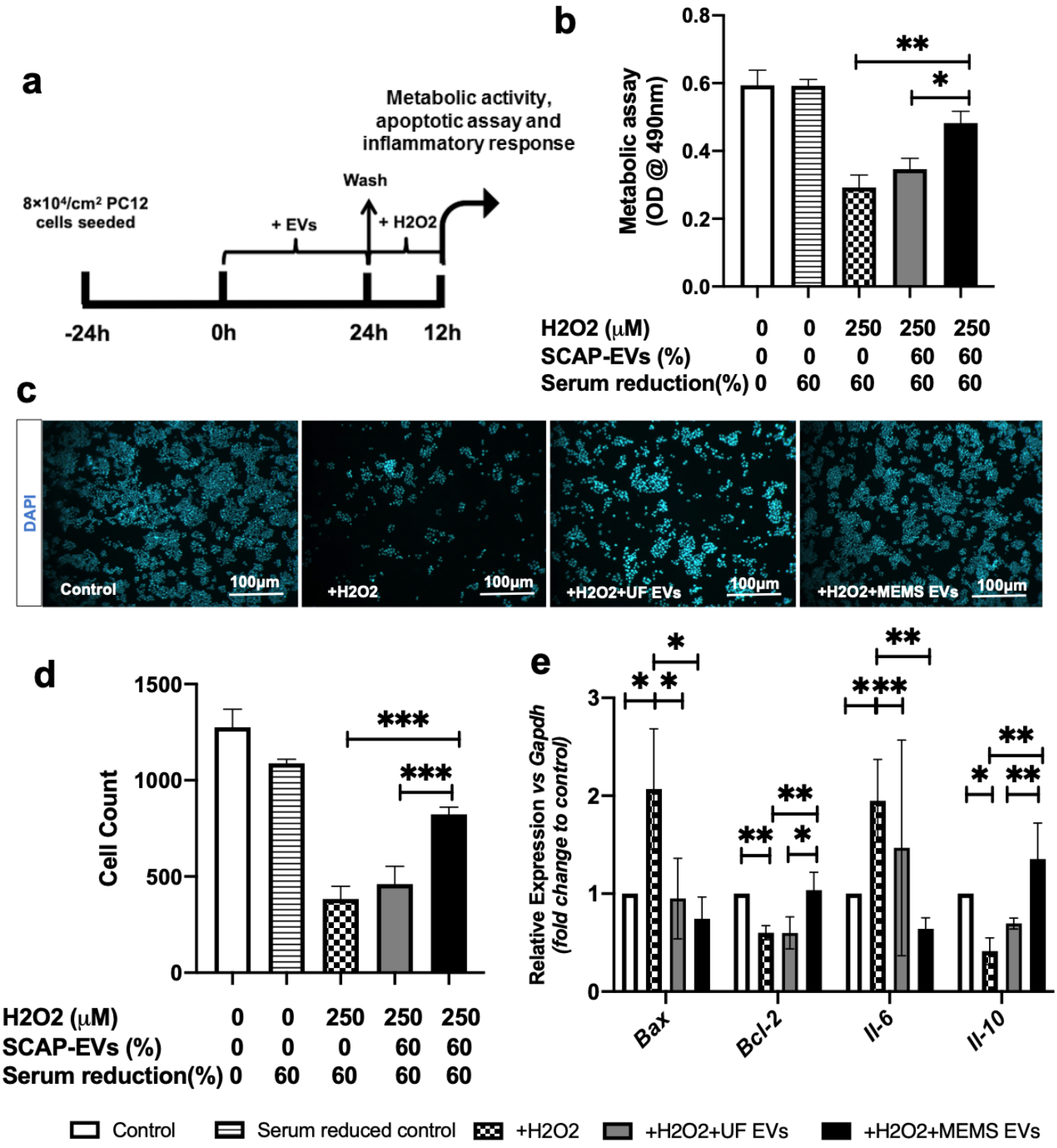

Figure 3

SCAP-EVs protect PC12 cells from H2O2-induced cytotoxicity in vitro. (a) Experimental design of in vitro study, (b) Metabolic activity (viability) of the PC12 cells that are received H2O2 and were under serum reduced condition alone or with SCAP-EVs pretreatment (n=3 per group). EVs were enriched by MEMS and UF approaches. Data are presented as mean ± SE. (c) Cell count of the PC12 cells that are received H2O2 and were under serum reduction condition alone or with enriched SCAP-EVs by MEMS and UF

approaches (n=3 per group). Data are presented as mean ± SE. (d) RT-qPCR analysis showing relative mRNA expression levels of Il-10, Il-6, Bax, and Bcl-2 compared to the negative control (n = 3 per group). Data are presented as mean ± SE. (e) PC12 cells morphology of untreated control and H2O2-induced group alone or with SCAP-EVs treatments that are enriched by MEMS or UF methods. *P < 0.05, **P< 0.01, ***P < 0.001. Abbreviation: SCAP, Stem cells from apical papilla; MEMS, Micro-electromechanical systems; UF, Ultrafiltration

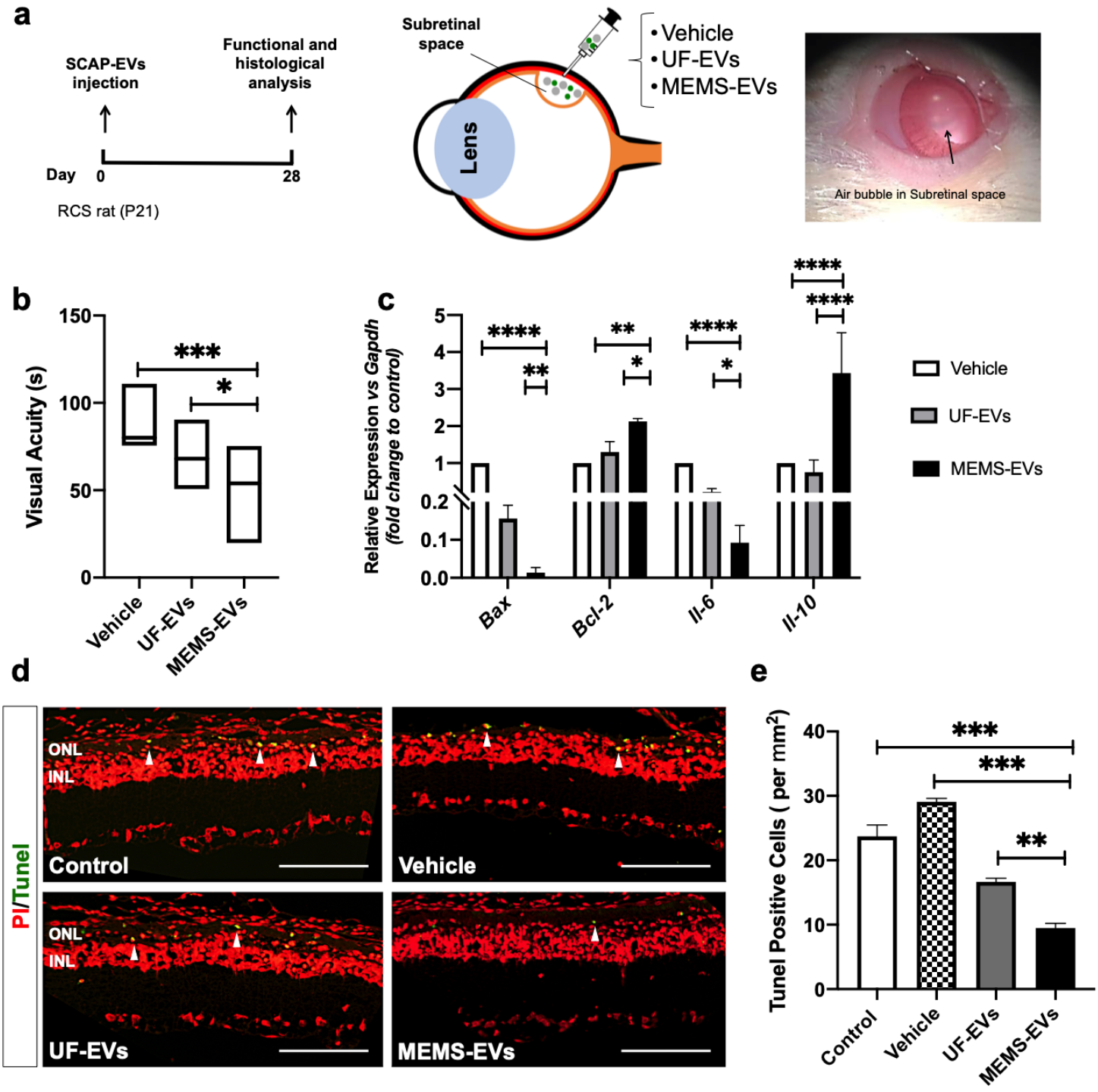

Figure 4

Implantation of SCAP-EVs preserves visual function in RCS rats (a) Experimental design of in vivo study (left panel); scheme illustrating the subretinal transplantation and the injected bubble to create the subretinal space (right panel), (b) Visual acuity measured through the visual cliff test in the vehicle, UF-EVs, and MEMS-EVs enriched groups on day 28 post-injection (n = 10 eyes per group). (c) RT-qPCR analysis showing relative mRNA expression levels of Il-10, Il-6, Bax and Bcl-2 compared to the vehicle (n = 3 per group). Data are presented as mean ± SE. (d) Apoptosis detection by TUNEL (green) and PI staining (red) in RCS retinas (inner nuclear layer, INL, and outer nuclear layer, ONL) of untreated control, vehicle, UF-EVs, and MEMS-EVs enriched groups at day 28 post-injection. Scale bar, 100 μm. (e) Numbers of apoptosis cells (TUNEL positive cells) in ONL were statistical analysed in untreated control, vehicle, UF EVs, and MEMS EVs enriched groups at day 28 post-injection (n = 3 per group) *P < 0.05, **P< 0.01, ***P< 0.001. Data are shown as mean ± SE. Abbreviations: SCAP, Stem cells from apical papilla; MEMS, Micro-electromechanical systems; UF, Ultrafiltration

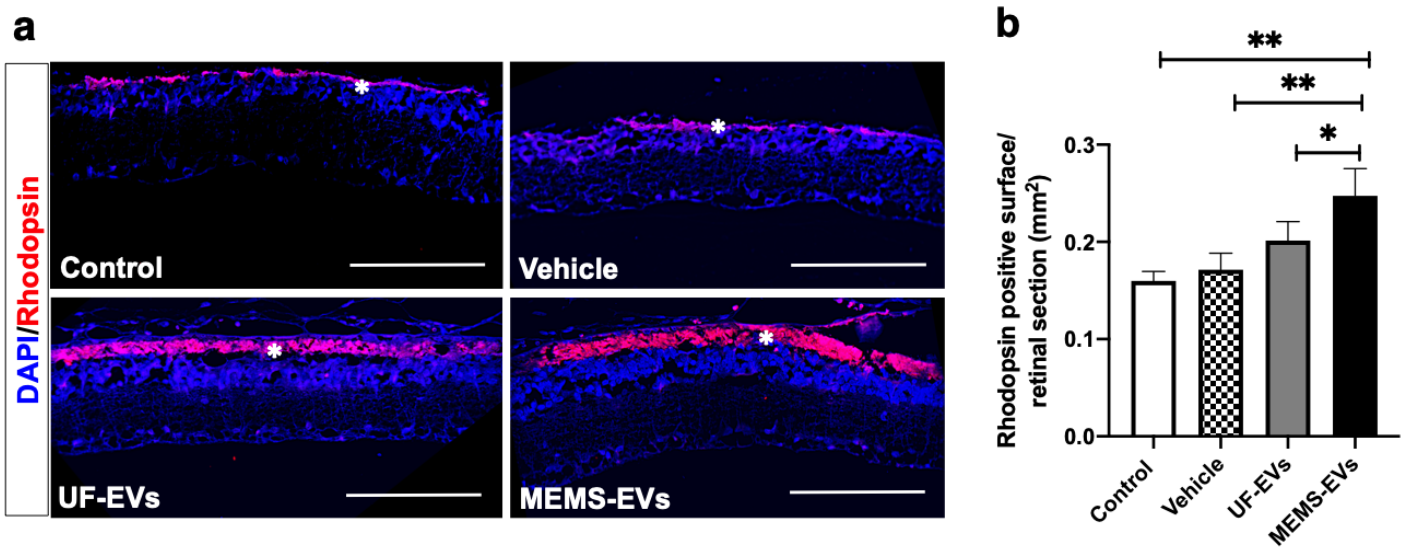

Figure 5

SCAP-EVs preserve the photoreceptor cell layer Immunofluorescence staining for rhodopsin (red) in sections of RCS rat retinas 28 days post-injection (postnatal 49 days). Nuclei were counterstained with DAPI (blue). (a) Panels show merge plus DAPI for untreated control, vehicle, UF-EVs, and MEMS-EVs injected groups. The asterisks indicate the position of the ONL. Scale bars, 100 μm. (b) Quantification of the rhodopsin-positive surface shows a significant increase in rod outer segment areas in MEMS-EVs treated group. (n = 3 per group) *P < 0.05, **P< 0.01, ***P< 0.001. Data are shown as mean ± SE. Abbreviation: ONL, outer nuclear layer; MEMS, Micro-electromechanical systems; UF, Ultrafiltration

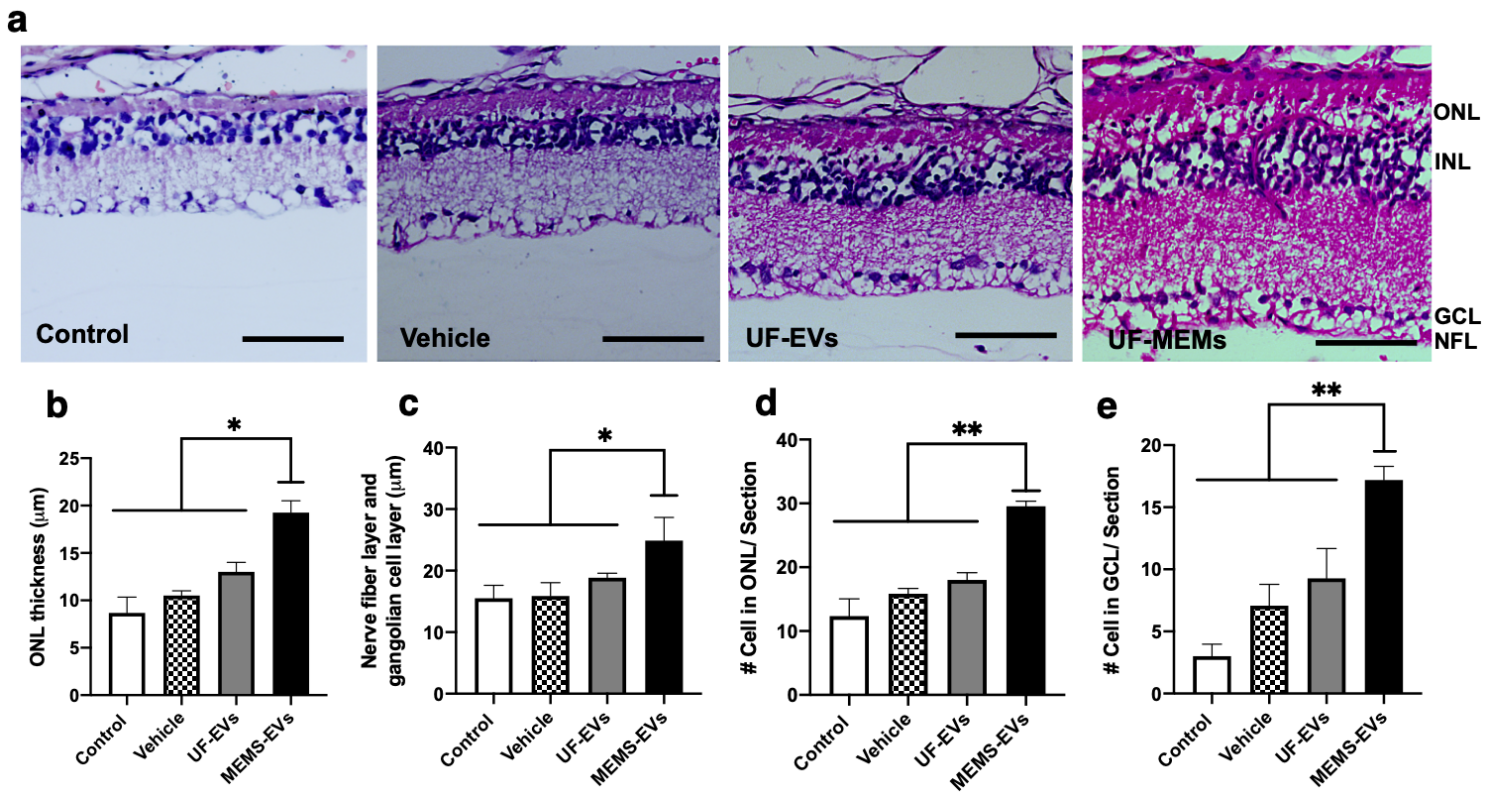

Figure 6

Measurement of the layer thickness and cell numbers in the outer nuclear layer (ONL) and ganglion cell /nerve fiber layer (GCL/NFL) (a) Light microscopy of hematoxylin eosin-stained RCS rat eyes show the retinal layers in untreated control, vehicle, UF-EVs, and MEMS-EVs enriched groups at day 28 post-injection (outer nuclear layer, ONL, inner nuclear layer, INL, ganglion cell layer, GCL, and nerve fiber layer, NFL). Scale bar, 100 μm. (b-c) quantification of ONL and GCL/NFL thickness measurements from all panels. (d) Cell numbers in the outer nuclear layer, (e) Cell numbers in the ganglion cell/nerve fiber layer (n = 3 per group) The injection site was taken as the reference point (three slices per retina; three fields per slice). *P < 0.05, **P< 0.01, ***P< 0.001. Data are shown as mean ± SE.

Supplementary Files

This is a list of supplementary files associated with this preprint. Click to download.

- SupplementaryinformationNat.Com.docx